# UNIVERSITÀ DI PARMA

## ARCHIVIO DELLA RICERCA

University of Parma Research Repository

One-armed spiral instability in neutron star mergers and its detectability in gravitational waves

This is the peer reviewd version of the followng article:

*Original*
One-armed spiral instability in neutron star mergers and its detectability in gravitational waves / Radice, David; Bernuzzi, Sebastiano; Ott, Christian D.. - In: PHYSICAL REVIEW D. - ISSN 2470-0010. - 94:6(2016). [10.1103/PhysRevD.94.064011]

*Availability:*
This version is available at: 11381/2814286 since: 2016-11-09T10:10:48Z

*Publisher:*

*Published*
DOI:10.1103/PhysRevD.94.064011

(Article begins on next page)

13 October 2022

# One-armed spiral instability in neutron star mergers and its detectability in gravitational waves

David Radice

*TAPIR, Walter Burke Institute for Theoretical Physics, California Institute of Technology,*
*1200 East California Boulevard, Pasadena, California 91125, USA*

Sebastiano Bernuzzi

*DiFeST, University of Parma, and INFN, I-43124 Parma, Italy*
*and TAPIR, Walter Burke Institute for Theoretical Physics, California Institute of Technology,*
*1200 East California Boulevard, Pasadena, California 91125, USA*

Christian D. Ott

*TAPIR, Walter Burke Institute for Theoretical Physics, California Institute of Technology,*
*1200 East California Boulevard, Pasadena, California 91125, USA*
*and Yukawa Institute for Theoretical Physics, Kyoto University, Kyoto 606-8502, Japan*

We study the development and saturation of the $m = 1$ one-armed spiral instability in remnants of binary neutron star mergers by means of high-resolution long-term numerical relativity simulations. Our results suggest that this instability is a generic outcome of neutron star mergers in astrophysically relevant configurations, including both "stiff" and "soft" nuclear equations of state. We find that, once seeded at merger, the $m = 1$ mode saturates within $\sim 10$ ms and persists over secular time scales. Gravitational waves emitted by the $m = 1$ instability have a peak frequency around 1–2 kHz and, if detected, they could be used to constrain the equation of state of neutron stars. We construct hybrid waveforms spanning the entire Advanced LIGO band by combining our high-resolution numerical data with state-of-the-art effective-one-body waveforms including tidal effects. We use the complete hybrid waveforms to study the detectability of the one-armed spiral instability for both Advanced LIGO and the Einstein Telescope. We conclude that the one-armed spiral instability is not an efficient gravitational wave emitter. Even under very optimistic assumptions, Advanced LIGO will only be able to detect the one-armed instability up to $\sim 3$ Mpc, which corresponds to an event rate of $10^{-7}$ yr$^{-1}$ to $10^{-4}$ yr$^{-1}$. Third-generation detectors or better will likely be required to observe the one-armed instability.

## I. INTRODUCTION

With the recent detection of gravitational waves (GWs) from a pair of merging black holes (BHs) [1], we have entered the era of GW astronomy. Binary neutron star (BNS) mergers are among the targets for the latest generation of laser-interferometer GW detectors—Advanced LIGO [2], Advanced Virgo [3], and KAGRA [4]. The direct detection of GWs from BNS mergers will reveal important aspects of the physics and astrophysics of NSs. Accurate phasing measurements of the GW signal during the late inspiral and merger in combination with robust theoretical predictions, e.g. Refs. [5–7], will provide accurate and nearly model-independent measurements of the masses and radii of NSs. This will help constrain the unknown physics of matter at supernuclear densities [8–12].

Recent observations of NSs with masses $\sim 2~M_\odot$ [13,14] in combination with the distribution of NS masses in Galactic binaries, which peaks at $\sim 1.35~M_\odot$ [15,16], suggests that the typical outcome of mergers is the formation of a stable remnant or of a hypermassive neutron star (HMNS). The latter is a metastable object that may survive for several tens of milliseconds before collapsing to a BH [17–25]. The merger remnant is an efficient GW emitter [25], and its gravitational radiation has discrete features (peaks) that could be used to provide additional constraints for the high-density part of the NS equation of state (EOS) [21,23,26–31]. However, the prospects for detecting this signal are diminished by its high frequency (2–4 kHz), which puts it outside of the maximum-sensitivity band of current GW detectors.

Recently, Refs. [32,33] considered the merger of spinning NSs on eccentric orbits and found that the resulting HMNS develops an $\ell = 2$, $m = 1$ one-armed spiral instability. Because of its $m = 1$ nature, this instability results in GW emission at half the frequency of the dominant $m = 2$ quadrupole mode, in a band of higher sensitivity for GW detectors. Similar instabilities have previously been identified in isolated differentially rotating NSs models [34,35] and in newly formed NSs in core collapse, e.g. Refs. [36–38]. There are also strong

indications of the presence of an $m = 1$ instability in previous simulations of spinning BNS mergers in quasi-circular orbits [39,40]. However, the impact of this instability for GW observation of BNS mergers is unclear—especially in the case of binaries with slowly rotating or nonrotating NSs in quasicircular orbit, which are presumably the most common.

In this paper, we present results of high-resolution numerical relativity (NR) simulations suggesting that the growth of an $m = 1$ instability is a generic outcome of BNS mergers and independent of the NS EOS. The one-armed spiral instability is only weakly damped and persists for several tens of milliseconds. However, we find that the one-armed spiral instability is an inefficient emitter of GWs. Their detection by current and near-future ground-based GW observatories is unlikely.

## II. NUMERICAL MODEL

We consider the GW-driven merger of two equal-mass ($q = M_A/M_B = 1$, $M_A = M_B = 1.35\,M_\odot$) neutron stars.

We construct quasicircular initial data in the conformally flat approximation assuming irrotational flow [41]. We treat NS matter as a perfect fluid and use two nuclear-theory-motivated piecewise polytropic EOSs [42] to close the equations of general relativistic (GR) hydrodynamics.

The EOSs that we employ are designed to fit the SLy [43] and MS1b [44] interaction models. With maximum nonrotating NS masses of $2.06\,M_\odot$ and $2.76\,M_\odot$, respectively, these two EOSs are representative choices of a "soft" and a "stiff" EOS. Thermal effects during the evolution are included using a gamma-law EOS component with $\Gamma_{\rm th} = 1.75$ [45]. The initial separation between the centers of the two NSs is 50 km, corresponding to approximately 9 and 11 orbits before merger for the MS1b and SLy models, respectively.

The simulations are performed using the Einstein Toolkit [46]. For the spacetime evolution we use the Z4c formulation [47] of Einstein's equations, implemented in the CTGamma code [48]. The GR hydrodynamics equations are solved using the high-order WhiskyTHC code [49–51]. Our numerical grid covers a cubical region of $2048\,M_\odot \simeq 3025$ km centered on the center of mass of the system. We enforce reflection symmetry across the $z = 0$ plane. We use the adaptive mesh refinement driver Carpet [52] to set up a grid consisting of seven refinement levels, with the finest ones being dynamically moved to follow the centroids of the two NSs. The innermost refinement level contains the NSs during the inspiral and the HMNS after merger. For each EOS we perform simulations with four different resolutions, having grid spacings, at the finest level, of $h = 0.25\,M_\odot$, $0.2\,M_\odot$, $0.15\,M_\odot$, and $0.1\,M_\odot$ (corresponding to approximately 369 m, 295 m, 222 m, and 148 m, respectively). For the time integration, we use a third-order strong stability-preserving Runge-Kutta

method [53] with the Courant-Friedrichs-Lewy factor set to 0.3. Finally, for our analysis, we consider up to the $\ell_{\rm max} = 4$ multipole of the gravitational radiation as extracted at future null infinity $\mathcal{J}^+$ using the gauge-invariant Cauchy characteristic extraction method developed by Ref. [54].

## III. ONE-ARMED SPIRAL INSTABILITY

The MS1b merger results in the creation of a stable NS, thanks to the large maximum mass supported by this EOS. The SLy binary forms a short-lived HMNS. We find the survival time to be resolution dependent, with the $0.25\,M_\odot$, $0.15\,M_\odot$, and $0.1\,M_\odot$ simulations showing apparent horizon formation at approximately 62.8 ms, 16.3 ms, and 14.9 ms after merger, respectively, defined as the time $t_0$ when the amplitude of the $\ell = 2$, $m = 2$ of the GW strain peaks. We do not continue the SLy $h = 0.2\,M_\odot$ simulation until BH formation.

In all our simulations we observe a spontaneous symmetry breaking of the system (e.g. Ref. [55]): small asymmetries due to the floating-point truncation error in our code are amplified by the turbulence generated by the Kelvin-Helmholtz instability in the contact region between the two stars [19,56,57]. This seeds physical odd-$m$ instabilities in the merger remnant.

We study the development of modes violating the 180° rotational symmetry ($\pi$ symmetry) of the initial data using a modal decomposition of the density on the equatorial plane,

$$P_i = \int_{\mathbb{R}^2} \rho W e^{-im\phi} \sqrt{\gamma}\mathrm{d}x\mathrm{d}y, \qquad (1)$$

where $\rho$ is the rest-mass density, $\gamma$ the determinant of the three-metric, and $W$ the Lorentz factor. We show the results of this analysis in Fig. 1. Similarly to what has been reported for spinning and/or eccentric BNSs mergers [32,33,39,40], we find that, at merger, several odd-$m$ modes are seeded. These grow exponentially until saturation is reached, within $\sim$10 ms. Among these, the $m = 1$ is one of the dominant modes and the most promising for GW detection. The $m = 3$ mode is also excited and relatively strong, especially with the SLy EOS, but its GW emission is at high frequency, out of the maximum-sensitivity band of GW detectors.

Figure 2 shows that for the MS1b binary with $h = 0.1\,M_\odot$, the one-armed spiral instability appears to develop similarly to the case of eccentric mergers [32,33]. Hydrodynamical vortices are formed at the time of merger (underdense regions in the first panel of Fig. 2). These vortices subsequently migrate toward the center where they join. This displaces the forming core of the merger remnant and triggers the development of a spiral arm. Note that some previous studies (e.g., Refs. [58,59]) suggested that toroidal (maximum density in a torus around the center) rather than spheroidal (centrally condensed) stellar structure was necessary for the one-armed instability to develop.
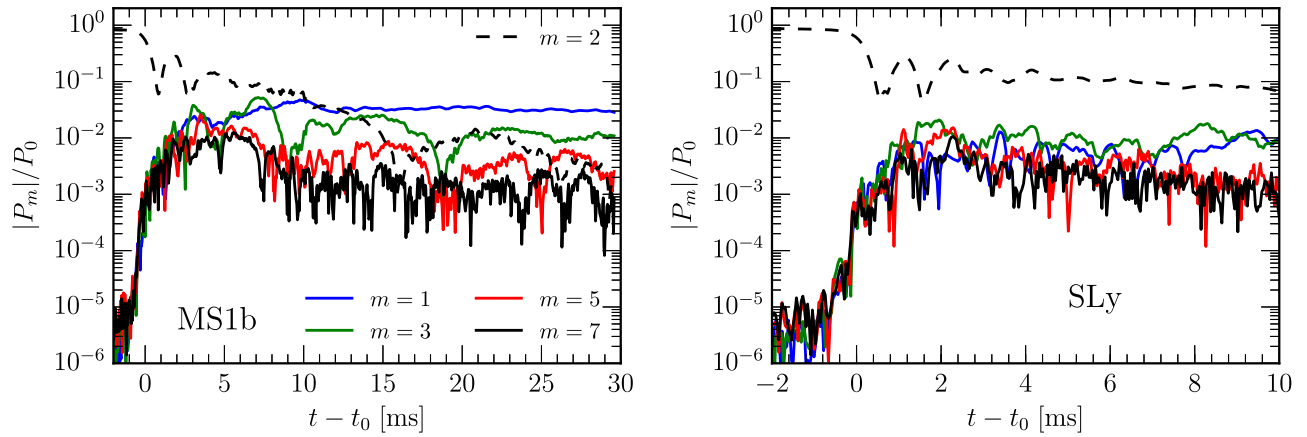
FIG. 1.    Normalized amplitudes of density modes on the equatorial plane. The symmetry-breaking odd-$m$ modes start to grow exponentially at the time the NSs enter into contact and saturate within few milliseconds.
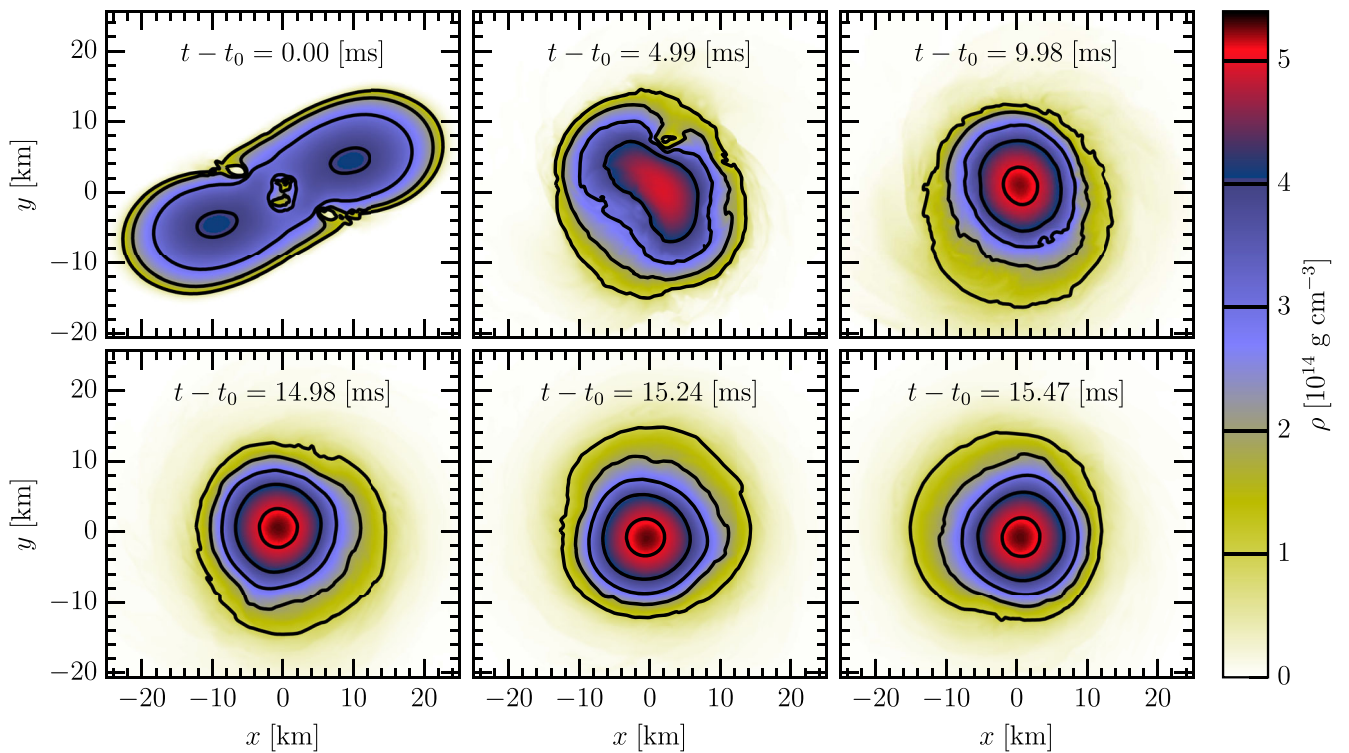


FIG. 2.    Color-coded rest-mass density in the orbital plane for our highest-resolution MS1b simulation at representative times after merger ($t_0$). In the upper panels: Merger and development of the $m = 1$ instability. In the bottom panels: Roughly half a cycle of the saturated spiral mode. The 180° rotational symmetry of the system is broken by hydrodynamic instabilities originating at the Kelvin-Helmholtz-unstable shear layer between the two stars shortly after merger. This causes the spiral mode to grow. Animations of the density in the orbital plane for both MS1b and SLy binaries are available as Supplemental Material [60].

We do not find this to be the case: while our models exhibit slightly off-center density peaks, they are globally spheroidal (cf. also Refs. [34,36–38]).

We estimate the strength of the one-armed spiral instability in an unambiguous way from the multipole decomposition of the GW energy and angular momentum fluxes, $L_{GW}$ and $\dot{J}_{GW}$, at $\mathcal{J}^+$. These are obtained from the spin $-2$ weighted spherical harmonics decomposition of the strain

$h_{\ell m}$ at future null infinity following Ref. [61]. The multipoles of the energy flux carried by GWs are

$$(L_{GW})_{\ell m} = (\dot{E}_{GW})_{\ell m} = \frac{1}{16\pi}|\dot{h}_{\ell m}|^2, \quad (2)$$

while the multipoles of the angular momentum flux are

$$(\dot{J}_{GW})_{\ell m} = \frac{m}{16\pi}\Im[h_{\ell m}\dot{h}_{\ell m}^*]. \quad (3)$$
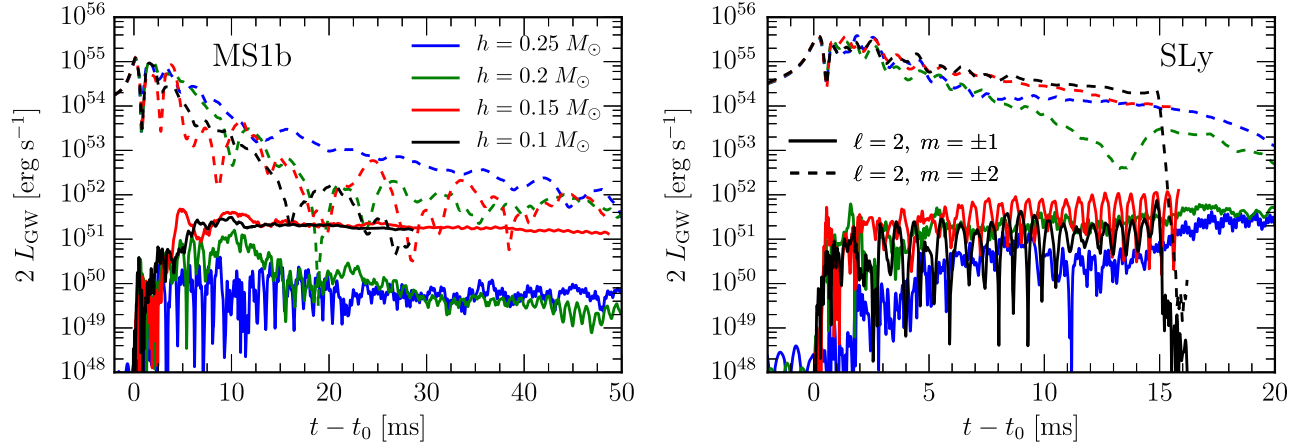
FIG. 3.    GW luminosity of the $\ell = 2$, $m = 2$ and $\ell = 2$, $m = 1$ modes for all simulations as a function of time from merger ($t - t_0$). The data are multiplied by a factor of 2 to account for the symmetry between positive and negative $m$. A contribution from the $m = 1$ mode is present in all simulations, especially at high resolution. GWs from the spiral mode are subdominant during most of the evolution, but show negligible damping.

We show the $\ell = 2$, $m = 1$ and $\ell = 2$, $m = 2$ quadrupole modes of the GW energy flux in Fig. 3. While the $\ell = 2$, $m = 2$ mode peaks at merger and then decays over a time scale of several milliseconds, the $m = 1$ mode grows after merger and saturates within a few milliseconds for both the MS1b and SLy binaries. In both cases, the mode appears not to be damped by hydrodynamical processes and persists for the entire duration of the simulations—i.e., up to 50 ms after merger in the MS1b case, or until BH formation in the SLy case.

The energy released in GWs by the one-armed spiral instability is several orders of magnitude smaller than that from the dominant $\ell = 2$, $m = 2$ mode after the merger. The $m = 1$ GW emission is not dynamically relevant for the evolution of the remnant in the first several tens of milliseconds. Even on secular timescales (for the MS1b binary), the $m = 1$ mode does not appear to be efficient at removing angular momentum from the remnant with $J/(2\dot{J}_{GW})_{\ell=2,m=1} \gtrsim 100$ s. For this reason, the $\ell = 2$, $m = 1$ mode is only very weakly damped by GW back-reaction. This is in contrast with the behavior of the dominant quadrupole mode, which is a highly efficient emitter of GWs and, for this reason, is strongly damped over a time scale of $\sim$10 ms [25]. After the $\ell = 2$, $m = 2$ mode has decayed, the $\ell = 2$, $m = 1$ mode becomes the most luminous mode. As shown in Fig. 3, this happens already 20 ms after merger in the highest-resolution MS1b simulation. The dominance of this mode over long time scales suggests that the one-armed spiral instability might leave some imprint on the GW signal if it survives for a sufficiently long time.

Figure 3 also shows that numerical viscosity in low-resolution simulations can prevent the one-armed spiral instability from fully developing. One could speculate that one of the reasons why this instability has gone undetected

for a long time is that it might have been suppressed in simulations performed at lower resolutions and/or using more dissipative numerical schemes than those used here. Another reason is the $\pi$ symmetry that was assumed in many previous simulations, which obviously prevents the instability completely. We also remark that, while the instability is very evident for stiff EOSs (Fig. 2), it is less so in the case of softer EOSs (e.g., in our SLy model). In the latter case, it is difficult to identify from the inspection of density color maps. A modal decomposition of the density distribution or an analysis of the GW multipoles is necessary to unambiguously reveal it.

## IV. HYBRID WAVEFORMS

We construct the complete GW signal in the Advanced LIGO band from our binaries by hybridizing our NR waveforms with the tidal effective-one-body (EOB) model presented in Ref. [6]. We generate EOB waveforms using a publicly available code [62], starting at a frequency of $\simeq$10 Hz, corresponding to $\simeq$18 minutes before merger, and extending up to the moment of merger [6,63]. We include multipoles up to $\ell = 4$. The resulting hybridized waveforms are publicly available [64].

We align NR and EOB data as in Ref. [6]. We use the difference between the two highest resolutions as a conservative estimate for the numerical uncertainty in the $\ell = 2$, $m = 2$ GW phase predicted by our simulations. The difference is less than 3 radians at merger and less than 0.3 radians in the time window where we perform the alignment with EOB. Excluding the lowest-resolution simulation, which appears not converged, we find better than third-order convergence in the phase and amplitude of the $\ell = 2$, $m = 2$ GW mode for both the MS1b and the SLy binaries until shortly before merger. This is similar to what was reported in Ref. [50]. As a consequence, the dephasing

between the NR and EOB waveforms is dominated by the residual orbital eccentricity, and the residuals are essentially flat until shortly before merger as in Ref. [6].

In order to be able to estimate the detectability of the one-armed spiral mode, we extend the $\ell = 2$, $m = 1$ GW signal of the MS1b binary to $\simeq 1$ s after merger using a simple damped sinusoid. This is justified by the fact that the $\ell = 2$, $m = 1$ GW signal from our MS1b simulations has a very stable instantaneous frequency and a narrow spectrum. Since the $\ell = 2$, $m = 1$ GW amplitude in our simulations shows low-frequency oscillations of unclear origin, we are not able to reliably estimate damping times from our data. Instead, we heuristically set the damping time of the $\ell = 2$, $m = 1$ mode in our hybrid waveform to 100 ms. This value is consistent with the amplitude evolution of the $h = 0.15 \, M_\odot$ run, but somewhat smaller than what could be inferred from the $h = 0.1 \, M_\odot$ data. However, other physical processes, such as neutrino cooling and angular momentum redistribution due to magnetoturbulence, will likely become dominant over such time scales [22] and might damp the one-armed spiral instability [65–67]. As a consequence, our estimate of the survival time of the $m = 1$ mode should constitute a reasonable upper limit.

## V. DETECTABILITY

In Fig. 4, we show the spectrum of the effective GW signals for the highest-resolution MS1b and SLy hybrid waveforms. For our analysis, we assume an optimistic distance of 10 Mpc to the source, an optimal sky location, and an edge-on orientation of the binary with respect to the detector, which is optimal for the detection of the $\ell = 2$, $m = 1$ mode. We also superimpose the sensitivity curves of Advanced LIGO in its zero-detuning high-laser-power configuration [68] and of the proposed ET [69,70].

We find the spectrum of the GW signal generated by the one-armed spiral instability to reach its maximum at a

frequency half that of the dominant quadrupole peak $f_2$. It is thus conceivable that the detection of GWs from the $m = 1$ instability could be used to constrain the NS EOS, since $f_2$ has been shown to encode properties of the EOS at high densities [21,26,28].

We quantify the detectability of the different components of the GW signal by computing optimal signal-to-noise ratios (SNRs), i.e., assuming an optimal detection template [71], for Advanced LIGO and ET using the hybrid waveforms obtained from the highest-resolution NR simulations. We compute the SNR integrals using $h_+(f)$ over the frequency windows 9 Hz $\leq f \leq$ 8192 Hz and 1 Hz $\leq f \leq$ 8192 Hz for Advanced LIGO and ET, respectively. We estimate low-frequency ($f \lesssim 12$ Hz) contributions to the SNR by extending the hybrid spectrum as a power law with index $-7/6$ at low frequencies [72]. The results of this analysis are reported in Table I.

Despite its large spectral peak amplitude, the detection of the $m = 1$ mode with current laser interferometers appears unlikely. Even at the relatively close distance of $D = 10$ Mpc, the optimal SNR for the $\ell = 2$, $m = 1$ GW mode of the hybrid MS1b waveform is only $\simeq 1.6$ for Advanced LIGO. For comparison, the threshold on the optimal SNR for detection is typically set to 8 [73]. This means that the one-armed spiral instability will be undetectable even for nearby events, and the $\ell = 2$, $m = 2$ GW mode appears much more promising for detecting postmerger GWs from BNS mergers. This is even more so for the short-lived merger remnant of the SLy binary.

Table I also reports the SNR accumulated by the $\ell = 2$, $m = 1$ GW mode over the 10 ms period after its amplitude has saturated. This value can be used to evaluate the dependency of the SNR on the survival time of the one-armed mode. Assuming that the $\ell = 2$, $m = 1$ GW mode survives for a time $T$ with no damping, the total SNR for the MS1b binary, for example, can be computed as
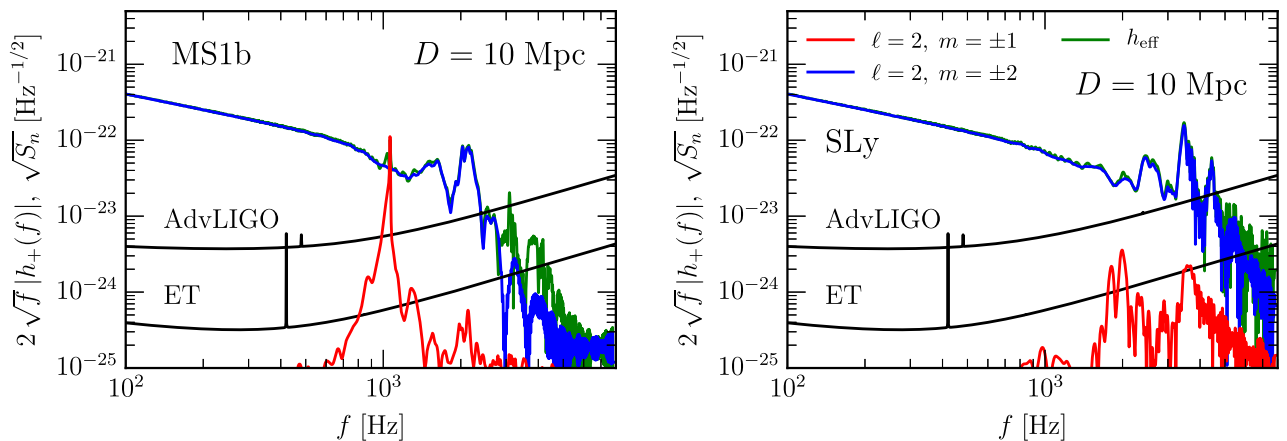


FIG. 4.   Spectrum of the effective GW signal seen edge-on from a distance of 10 Mpc. We show the spectrum of the hybrid waveforms constructed from the highest-resolution data and the noise curves of Advanced LIGO and the Einstein Telescope (ET). The $\ell = 2$, $m = 1$ spectrum is mostly concentrated in a narrow maximum located at half of the frequency of the $\ell = 2$, $m = 2$ peak.

TABLE I.   Single-detector SNRs of different components of the GW signal for the MS1b and SLy binaries at a distance of 10 Mpc, seen edge-on, and computed assuming optimal sky location. We quote the SNR of the entire waveform (all multipoles up to $\ell = 4$), the SNR of the $\ell = 2$, $m = 1$ mode $SNR_{2,1}$, and the SNR accumulated by the $\ell = 2$, $m = 1$ mode in a window of 10 ms after merger $SNR_{2,1}^{10\,ms}$. For the time windowing, we use $10\,ms \leq t - t_0 \leq 20\,ms$ for the MS1b binary and $3\,ms \leq t - t_0 \leq 13\,ms$ for the SLy binary. Finally, we also give the SNR for the $\ell = 2$, $m = 2$ mode computed using only the high-frequency ($f \geq 1$ kHz) component of the GW signal $SNR_{2,2}^{f \geq 1\,kHz}$.

| Det. | Binary | SNR | $SNR_{2,1}$ | $SNR_{2,1}^{10\,ms}$ | $SNR_{2,2}^{f \geq 1\,kHz}$ |
|---|---|---|---|---|---|
| LIGO | MS1b-M135 | 169.4 | 1.6 | 0.62 | 5.4 |
| LIGO | SLy-M135 | 169.5 | 0.1 | 0.09 | 6.9 |
| ET | MS1b-M135 | 2460.5 | 14.4 | 5.86 | 47.4 |
| ET | SLy-M135 | 2461.6 | 1.0 | 0.80 | 61.3 |

$$SNR = 0.62 \left( \frac{10\,Mpc}{D} \right) \left( \frac{T}{10\,ms} \right)^{1/2}. \qquad (4)$$

Our fiducial case, with a damping time scale of 100 ms, would correspond to an *effective* survival time $T_{eff} \simeq 67$ ms.

We also remark that our analysis refers to the case of binaries seen edge-on. In the face-on case, the SNR for the $\ell = 2$, $m = 2$ mode is twice as large, while the $\ell = 2$, $m = 1$ mode is completely suppressed.

## VI. DISCUSSION

In combination with previous studies by others [32,33,39,40], our results for equal-mass, irrotational BNS mergers from quasicircular orbits strongly suggest that the one-armed spiral instability is a generic outcome of the merger of two NSs. As we demonstrate in the cases of both soft and stiff EOSs, even tiny asymmetries, necessarily of numerical origin for exactly equal-mass systems, but expected in any astrophysical configuration, are sufficient to trigger the growth of this instability. Once seeded at the time of merger, the one-armed spiral instability quickly grows into a large-scale $m = 1$ spiral density perturbation, which saturates within a time scale of $\sim 10$ ms. Our results are supported by the analysis of well-defined gauge-invariant quantities at $\mathcal{J}^+$, and by a resolution study.

We find that GWs excited by the $m = 1$ mode carry relatively little energy and angular momentum as compared to those of the dominant $m = 2$ mode. As a consequence, the $m = 1$ mode is very weakly damped and may persist over secular time scales, while the $m = 2$ mode decays over a time scale of $\sim 10$ ms.

The characteristic frequency of the GW emitted by the one-armed spiral instability encodes important aspects of the NS EOS. Unfortunately, as our analysis shows, the direct observation of GWs from the $m = 1$ mode by the current GW detectors appears unlikely. We find that, even using an optimal SNR detection threshold as low as 5, Advanced LIGO at its design sensitivity will be able to detect optimally oriented sources only out to $\sim 3$ Mpc.

The expected event rate for BNS mergers in this volume is only $10^{-7}$ yr$^{-1}$ to $10^{-4}$ yr$^{-1}$ [73]. This picture could only change if the $\ell = 2$, $m = 1$ mode is somehow able to survive for many hundreds of milliseconds with no significant damping. However, the decay rates we observe in our simulations seem to exclude this possibility. In contrast, we find a horizon distances for the postmerger $m = 2$ mode of $\sim 20$ Mpc and $\sim 27$ Mpc for the MS1b and SLy binaries, respectively, assuming optimal orientation for the $\ell = 2$, $m = 2$ mode. This is in agreement with the more careful analysis of results of conformally flat simulations by Ref. [30]. GWs from the one-armed spiral instability will be a target for third-generation detectors, such as ET. For the latter, we find an optimal SNR for the $\ell = 2$, $m = 1$ mode of our highest-resolution MS1b hybrid waveform of $\simeq 14.4$ at 10 Mpc using the ET-D sensitivity curve [70]. This would put the horizon for the detection of an optimally oriented source at $\sim 29$ Mpc. This corresponds to an increase in the event rate by a factor of $10^3$ with respect to that of Advanced LIGO.

The most important limitation of our study is the omission of magnetohydrodynamic effects. Very strong magnetic fields have been shown to be able to suppress this instability in isolated NSs [66]. Muhlberger *et al.* [67], however, found that large-scale hydrodynamical instabilities in isolated differentially rotating NSs are not affected and in some cases are even amplified by the presence of magnetic fields over a large range of magnetic field strengths.

As a side product of the present study, we constructed, for the first time, high-quality hybrid waveforms employing state-of-the-art analytical models and high-resolution high-order NR data. These waveforms are publicly available [64].

---

[1] B. P. Abbott, R. Abbott, T. D. Abbott, M. R. Abernathy, F. Acernese, K. Ackley, C. Adams, T. Adams, P. Addesso, R. X. Adhikari *et al.*, Phys. Rev. Lett. **116**, 061102 (2016).

[2] J. Aasi, B. P. Abbott, R. Abbott, T. Abbott, M. R. Abernathy, K. Ackley, C. Adams, T. Adams, P. Addesso *et al.* (LIGO Scientific Collaboration), Classical Quantum Gravity **32**, 115012 (2015).

[3] F. Acernese *et al.* (VIRGO), Classical Quantum Gravity **32**, 024001 (2015).

[4] Y. Aso, Y. Michimura, K. Somiya, M. Ando, O. Miyakawa, T. Sekiguchi, D. Tatsumi, and H. Yamamoto (KAGRA), Phys. Rev. D **88**, 043007 (2013).

[5] K. Hotokezaka, K. Kyutoku, H. Okawa, and M. Shibata, Phys. Rev. D **91**, 064060 (2015).

[6] S. Bernuzzi, A. Nagar, T. Dietrich, and T. Damour, Phys. Rev. Lett. **114**, 161103 (2015).

[7] K. Hotokezaka, K. Kyutoku, Y.-i. Sekiguchi, and M. Shibata, Phys. Rev. D **93**, 064082 (2016).

[8] T. Damour, A. Nagar, and L. Villain, Phys. Rev. D **85**, 123007 (2012).

[9] J. S. Read, L. Baiotti, J. D. E. Creighton, J. L. Friedman, B. Giacomazzo, K. Kyutoku, C. Markakis, L. Rezzolla, M. Shibata, and K. Taniguchi, Phys. Rev. D **88**, 044042 (2013).

[10] W. Del Pozzo, T. G. F. Li, M. Agathos, C. Van Den Broeck, and S. Vitale, Phys. Rev. Lett. **111**, 071101 (2013).

[11] B. D. Lackey and L. Wade, Phys. Rev. D **91**, 043002 (2015).

[12] M. Agathos, J. Meidam, W. Del Pozzo, T. G. F. Li, M. Tompitak, J. Veitch, S. Vitale, and C. Van Den Broeck, Phys. Rev. D **92**, 023012 (2015).

[13] P. Demorest, T. Pennucci, S. Ransom, M. Roberts, and J. Hessels, Nature (London) **467**, 1081 (2010).

[14] J. Antoniadis *et al.*, Science **340**, 1233232 (2013).

[15] J. M. Lattimer, Annu. Rev. Nucl. Part. Sci. **62**, 485 (2012).

[16] B. Kiziltan, A. Kottas, M. De Yoreo, and S. E. Thorsett, Astrophys. J. **778**, 66 (2013).

[17] T. W. Baumgarte, S. L. Shapiro, and M. Shibata, Astrophys. J. Lett. **528**, L29 (2000).

[18] M. Shibata and K. Taniguchi, Phys. Rev. D **73**, 064027 (2006).

[19] L. Baiotti, B. Giacomazzo, and L. Rezzolla, Phys. Rev. D **78**, 084033 (2008).

[20] Y. Sekiguchi, K. Kiuchi, K. Kyutoku, and M. Shibata, Phys. Rev. Lett. **107**, 051102 (2011).

[21] A. Bauswein and H. T. Janka, Phys. Rev. Lett. **108**, 011101 (2012).

[22] K. Hotokezaka, K. Kiuchi, K. Kyutoku, T. Muranushi, Y. Sekiguchi, M. Shibata, and K. Taniguchi, Phys. Rev. D **88**, 044026 (2013).

[23] K. Takami, L. Rezzolla, and L. Baiotti, Phys. Rev. Lett. **113**, 091104 (2014).

[24] C. Palenzuela, S. L. Liebling, D. Neilsen, L. Lehner, O. L. Caballero, E. O'Connor, and M. Anderson, Phys. Rev. D **92**, 044045 (2015).

[25] S. Bernuzzi, D. Radice, C. D. Ott, L. F. Roberts, P. Moesta, and F. Galeazzi, Phys. Rev. D **94**, 024023 (2016).

[26] A. Bauswein, N. Stergioulas, and H.-T. Janka, Phys. Rev. D **90**, 023002 (2014).

[27] K. Takami, L. Rezzolla, and L. Baiotti, Phys. Rev. D **91**, 064001 (2015).

[28] S. Bernuzzi, T. Dietrich, and A. Nagar, Phys. Rev. Lett. **115**, 091101 (2015).

[29] F. Foucart, R. Haas, M. D. Duez, E. O'Connor, C. D. Ott, L. Roberts, L. E. Kidder, J. Lippuner, H. P. Pfeiffer, and M. A. Scheel, Phys. Rev. D **93**, 044019 (2016).

[30] J. A. Clark, A. Bauswein, N. Stergioulas, and D. Shoemaker, Classical Quantum Gravity **33**, 085003 (2016).

[31] R. De Pietri, A. Feo, F. Maione, and F. Löffler, Phys. Rev. D **93**, 064047 (2016).

[32] V. Paschalidis, W. E. East, F. Pretorius, and S. L. Shapiro, Phys. Rev. D **92**, 121502 (2015).

[33] W. E. East, V. Paschalidis, F. Pretorius, and S. L. Shapiro, Phys. Rev. D **93**, 024011 (2016).

[34] S. Ou and J. E. Tohline, Astrophys. J. **651**, 1068 (2006).

[35] G. Corvino, L. Rezzolla, S. Bernuzzi, R. De Pietri, and B. Giacomazzo, Classical Quantum Gravity **27**, 114104 (2010).

[36] C. D. Ott, S. Ou, J. E. Tohline, and A. Burrows, Astrophys. J. Lett. **625**, L119 (2005).

[37] C. D. Ott, H. Dimmelmeier, A. Marek, H.-T. Janka, I. Hawke, B. Zink, and E. Schnetter, Phys. Rev. Lett. **98**, 261101 (2007).

[38] T. Takiwaki, K. Kotake, and Y. Suwa, Mon. Not. R. Astron. Soc. **461**, L112 (2016).

[39] S. Bernuzzi, T. Dietrich, W. Tichy, and B. Brügmann, Phys. Rev. D **89**, 104021 (2014).

[40] W. Kastaun and F. Galeazzi, Phys. Rev. D **91**, 064027 (2015).

[41] E. Gourgoulhon, P. Grandclement, K. Taniguchi, J.-A. Marck, and S. Bonazzola, Phys. Rev. D **63**, 064029 (2001).

[42] J. S. Read, B. D. Lackey, B. J. Owen, and J. L. Friedman, Phys. Rev. D **79**, 124032 (2009).

[43] F. Douchin and P. Haensel, Astron. Astrophys. **380**, 151 (2001).

[44] H. Müller and B. D. Serot, Nucl. Phys. **A606**, 508 (1996).

[45] A. Bauswein, H.-T. Janka, and R. Oechslin, Phys. Rev. D **82**, 084043 (2010).

[46] F. Löffler *et al.*, Classical Quantum Gravity **29**, 115001 (2012).

[47] S. Bernuzzi and D. Hilditch, Phys. Rev. D **81**, 084003 (2010).

[48] D. Pollney, C. Reisswig, E. Schnetter, N. Dorband, and P. Diener, Phys. Rev. D **83**, 044045 (2011).

[49] D. Radice and L. Rezzolla, Astron. Astrophys. **547**, A26 (2012).

[50] D. Radice, L. Rezzolla, and F. Galeazzi, Mon. Not. R. Astron. Soc. **437**, L46 (2014).

[51] D. Radice, L. Rezzolla, and F. Galeazzi, Classical Quantum Gravity **31**, 075012 (2014).

[52] E. Schnetter, S. Haley, and I. Hawke, Classical Quantum Gravity **21**, 1465 (2004).

[53] S. Gottlieb, C. Shu, and E. Tadmor, SIAM Rev. **43**, 89 (2001).

[54] C. Reisswig, N. T. Bishop, D. Pollney, and B. Szilágyi, Phys. Rev. Lett. **103**, 221101 (2009).

[55] J. D. Crawford and E. Knobloch, Annu. Rev. Fluid Mech. **23**, 341 (1991).

[56] S. Rosswog and M. B. Davies, Mon. Not. R. Astron. Soc. **334**, 481 (2002).

[57] M. Anderson, E. W. Hirschmann, L. Lehner, S. L. Liebling, P. M. Motl, D. Neilsen, C. Palenzuela, and J. E. Tohline, Phys. Rev. Lett. **100**, 191101 (2008).

[58] J. M. Centrella, K. C. B. New, L. L. Lowe, and J. D. Brown, Astrophys. J. Lett. **550**, L193 (2001).

[59] M. Saijo, T. W. Baumgarte, and S. L. Shapiro, Astrophys. J. **595**, 352 (2003).

[60] See Supplemental Material at http://link.aps.org/supplemental/10.1103/PhysRevD.94.064011 for Visualizations of the density in the orbital plane.

[61] S. Bernuzzi, A. Nagar, M. Thierfelder, and B. Brugmann, Phys. Rev. D **86**, 044030 (2012).

[62] https://eob.ihes.fr.

[63] S. Bernuzzi, A. Nagar, S. Balmelli, T. Dietrich, and M. Ujevic, Phys. Rev. Lett. **112**, 201101 (2014).

[64] D. Radice, S. Bernuzzi, and C. D. Ott, Binary Neutron Star Merger Waveforms, doi:10.5281/zenodo.46733 (2016).

[65] W. Fu and D. Lai, Mon. Not. R. Astron. Soc. **413**, 2207 (2011).

[66] L. Franci, R. De Pietri, K. Dionysopoulou, and L. Rezzolla, Phys. Rev. D **88**, 104028 (2013).

[67] C. D. Muhlberger, F. H. Nouri, M. D. Duez, F. Foucart, L. E. Kidder, C. D. Ott, M. A. Scheel, B. Szilágyi, and S. A. Teukolsky, Phys. Rev. D **90**, 104014 (2014).

[68] D. Shoemaker (LIGO Scientific Collaboration), Technical Report No. LIGO-T0900288-v3, 2010, https://dcc.ligo.org/cgi-bin/DocDB/ShowDocument?docid=t0900288.

[69] M. Punturo, M. Abernathy, F. Acernese, B. Allen, N. Andersson, K. Arun, F. Barone, B. Barr, M. Barsuglia, M. Beker et al., Classical Quantum Gravity **27**, 084007 (2010).

[70] S. Hild, M. Abernathy, F. Acernese, P. Amaro-Seoane, N. Andersson, K. Arun, F. Barone, B. Barr, M. Barsuglia, M. Beker et al., Classical Quantum Gravity **28**, 094013 (2011).

[71] B. S. Sathyaprakash and B. F. Schutz, Living Rev. Relativ. **12** (2009).

[72] M. Maggiore, Gravitational Waves: Theory and Experiments (Oxford University Press, Oxford, 2008), https://cds.cern.ch/record/1080850.

[73] J. Abadie, B. P. Abbott, R. Abbott, M. Abernathy, T. Accadia, F. Acernese, C. Adams, R. Adhikari, P. Ajith, B. Allen et al., Classical Quantum Gravity **27**, 173001 (2010).